PRESSURE AND STRESS DISTRIBUTIONS DUE TO A SUBMERGED IMPINGING JET

Gregory J. Hanson[1] A. M. ASCE Kerry M. Robinson[1] Darrel M. Temple[1] M. ASCE

ABSTRACT

This investigation examines the pressure and shear stress distribution at a smooth planar boundary in the impingement region of a submerged vertical jet in water. The mean pressure and shear stress distributions are similar to those measured in air jet studies. An empirical relationship is developed for describing the shear stress distribution along the entire planar boundary in the impingement region.

INTRODUCTION

The flow characteristics of a circular submerged jet impinging normally on a smooth boundary has been investigated by Poreh and Cermak (1959), Beltaos and Rajaratnam (1974), and Viegas and Borges (1986). With the exception of Poreh and Cermak (1959), who conducted their test in water, these studies have been conducted with air jets.

The impinging circular jet has four zones of flow as depicted in Fig. 1. Zone 1 is described as the "zone of flow establishment" which extends about nine jet diameters from the origin (Poreh and Cermak, 1959). Zone 2 is defined as the "zone of established flow." Zone 3 is the "deflection zone" in which the jet impacts the smooth planar surface and transitions from a vertical jet to a horizontal wall jet. A stagnation point occurs along the centerline of the jet at the planar boundary. At the stagnation point, pressure is at maximum and shear stress is zero. Zone 4 is defined as the "wall jet zone" in which the flow of the jet is parallel to the planar boundary.

---

[1] Res. Hydr. Engr. USDA, ARS, Hydraulic Engineering Research Unit, 1301 N. Western, Stillwater, OK 74075. In cooperation with the Oklahoma Ag. Exp. Station.

To define the pressure and shear stress distributions along the planar boundary in the vicinity of the impingement region of the jet, researchers have resorted to semi-empirical relationships developed from experimental techniques. The objectives of this study were to measure the pressures and hydraulic stresses along the boundary in the vicinity of the impingement region, zones 3 and 4. The objectives also included the comparison of the relationships derived in air jet studies with the submerged water jet results, and the development of relationships that describe these particular results more precisely.

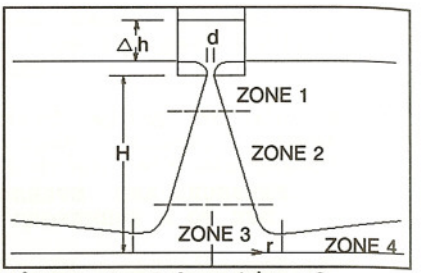

Figure 1 Schematic of impinging jet.

EXPERIMENTAL EQUIPMENT

Model

A submerged vertical water jet was produced by a 13 mm diameter, d, nozzle supplied by a constant head tank. The jet discharged into the center of a 0.61 m diameter tank which also acted as a weir to submerge the jet. The bottom of the tank was constructed of a 1.40 by 0.72-m by 38-mm thick plexiglass sheet. The center of the plexiglass sheet had a 3.2-mm hole for a pressure tap and for a flush mounted hot-film sensor to measure boundary shear stress. The sheet allowed movement of the transducer and sensor to various radial locations, r, beneath the impinging jet. An inflatable seal was used to prevent leakage between the tank and sheet. The height, H, of the nozzle from the boundary was set at 215 mm; therefore, the H/d ratio was 16.5. Pressure taps were placed in the side of the tank and upstream of the nozzle to allow observation of the pressure differential, Δh.

Instrumentation

A temperature compensated pressure transducer was used to measure pressure fluctuations. A flush mounted constant temperature anemometer probe was used to measure the boundary shear stress. A thermistor thermometer was used to monitor calibration loop and model temperature. A digital oscilloscope was used to receive and record the stress, temperature, and pressure signals.

Procedure

The pressure transducer was calibrated before and after each model run. For the model run, voltage

readings were taken at predetermined radial locations from the stagnation point of the jet for a range of differential heads, Δh (Table 1). Radial distances ranged from 0 to 216 mm which was an r/H range of 0 to 1.0.

A test run for measuring the boundary shear stress involved calibrating the hot film probe in a pipe loop before and after each model run. For the model run, the probe was mounted in the plexiglass sheet and voltage readings were taken at predetermined radial locations for a range of differential heads, Δh (Table 1).

RESULTS

The pressure transducer calibrations produced a linear relationship between time-averaged pressure and voltage, V. Calibration curves were fit with a regression equation of the form Pressure = a(V)+b (Fig. 2).

The hot-film probe calibrations produced a nonlinear relationship between time-averaged stress, τ, and voltage, V. Calibration curves were developed to eliminate non-linear biasing. A least squares optimization procedure was used to fit the calibration voltage data with an equation of the form $\tau = a(V^b)+c$ (Fig. 3). The hot-film probe was sensitive to various factors such as probe fouling, impact, and temperature drift. If the summation of the square of error was greater than 0.015, the calibrations were considered unacceptable, and the test was repeated.

The pressure, ΔP_w, and stress, τ_o, measurements were taken at locations in the model, based on the radial distance from the centerline of the jet. Pressure and stress distributions are provided (Figs. 4 and 5) for combinations of radial position and differential head. The pressure measurements at the boundary are represented as a pressure differential, ΔP_w, between the measured pressure and the hydrostatic pressure.

Beltaos and Rajaratnam (1974) developed a semi-empirical relationship for the peak values of pressure at r/H=0:

$$\Delta P_s = C\left(\frac{\rho U_o^2}{(H/d)^2}\right) \qquad \text{Eq. 1}$$

and for the pressure distribution at the boundary:

$$\frac{\Delta P_w}{\Delta P_s} = e^{-114\,(r/H)^2} \qquad \text{Eq. 2}$$

The value of C (Eq. 1) determined from the present study was 27.8 (Fig. 6). Beltaos and Rajaratnam (1974), working in air, obtained a value of 25.0 and indicated

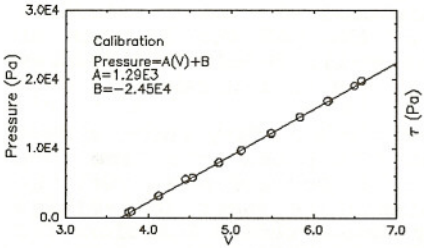

Figure 2 Pressure calibration

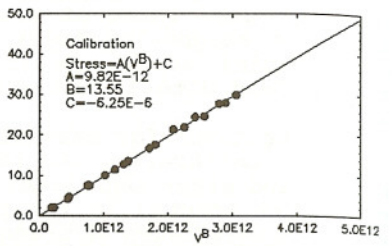

Figure 3 Shear stress calibration

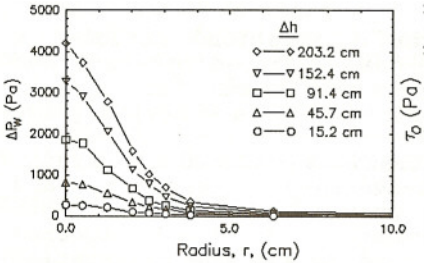

Figure 4 Measured pressure distributions

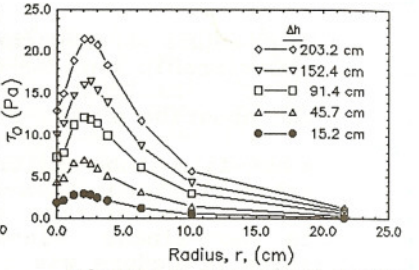

Figure 5 Measured shear stress distributions

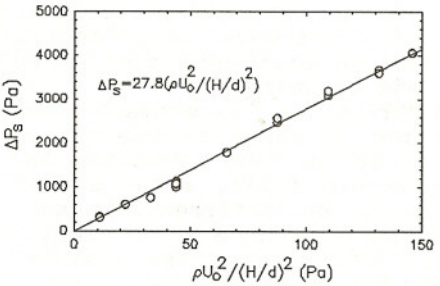

Figure 6 Maximum pressure relationship

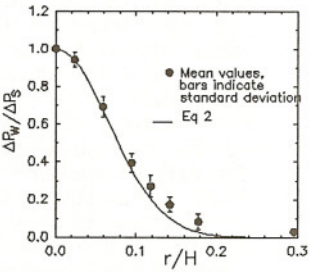

Figure 7 Dimensionless pressure profiles

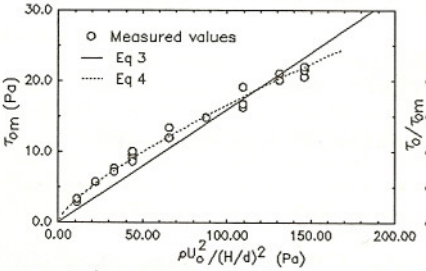

Figure 8 Maximum stress relationship

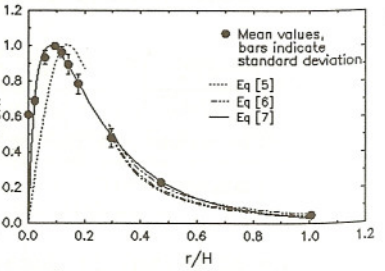

Figure 9 Dimensionless shear stress profiles

that the theoretical value was 28.5. Poreh and Cermak (1959) obtained a value of 30.2 working in water. Equation 2 is compared with experimental results of this study in Fig. 7.

The relationship for the maximum shear stress, τ_{om}, developed by Beltaos and Rajaratnam (1974) was:

$$\tau_{om} = 0.16 \left(\frac{\rho U_o^2}{(H/d)^2} \right) \qquad \text{Eq. 3}$$

For practical purposes, Eq. 3 estimates the measured stresses reasonably well, although a more accurate relationship of the experimental results is the power function (Fig. 8):

$$\tau_{om} = 0.56 \left(\frac{\rho U_o^2}{(H/d)^2} \right)^{0.74} \qquad \text{Eq. 4}$$

Beltaos and Rajaratnam (1974) also developed a semi-empirical relationship for describing the shear stress distribution along the boundary for $r/H < 0.22$:

$$\frac{\tau_o}{\tau_{om}} = 0.18 \left(\frac{1-e^{-114\,(r/H)^2}}{r/H} \right) - 9.43\,(r/H)\, e^{-114\,(r/H)^2} \qquad \text{Eq. 5}$$

Viegas and Borges (1986) developed a semi-empirical relationship for describing the shear stress distribution for $r/H > 0.22$ which combined with Eq. 3 yields:

$$\frac{\tau_o}{\tau_{om}} = 0.67\,(R_o)^{-0.256}\,(r/H)^{-0.878 R_o^{0.078}} \qquad \text{Eq. 6}$$

where R_o is the Reynolds number based on nozzle velocity and diameter. This equation indicates that stress observed at the boundary in zone 4 is weakly dependent on the Reynolds number. The measured shear stress in this study was also observed to be weakly dependent on the Reynolds number in zone 4.

An empirical equation was developed to describe the stress distribution for this study from $r/H = 0$ to $r/H = 1$:

$$\frac{\tau_o}{\tau_{om}} = 66.5\,(r/H)\, e^{-7.68\,(r/H)^{0.6}} \qquad \text{Eq. 7}$$

This equation was developed without incorporating the dependence on Reynolds number in order to keep it simple and yet describe the shape of the distribution.

A comparison of the tests results and Eqs. 5, 6, and 7 is shown in Fig. 9. The peak shear stress determined from experimental results appeared to be slightly closer to the stagnation point than that determined from the air jet studies. Theoretically, the shear stress is zero at the stagnation point ($r/H = 0$), whereas experimental results indicate that the shear stress at $r/H = 0$ is

$0.6\tau_{om}$. The empirical relationship, Eq. 7, describes the stress distribution for the entire reach from r/H = 0 to 1 fairly well and eliminates the need for the two part approach as developed in the air jet studies.

SUMMARY

Pressure and shear stress distributions at a smooth planar boundary in the impingement region of a submerged vertical water jet were found to be similar to those measured in submerged vertical air jets. Relationships were developed for the maximum pressure, the pressure distribution, the maximum shear stress, and the shear stress distribution.

REFERENCES

Beltaos S., and N. Rajaratnam (1974). "Impinging Circular Turbulent Jets," Journal of the Hydraulics Division, American Society of Civil Engineers, 100 (HY10), 1313-1328.

Poreh, M. and J. E. Cermak (1959). "Flow Characteristics of a Circular Submerged Jet Impinging Normally on a Smooth Boundary," Proceedings of the Sixth Midwestern Conference on Fluid Mechanics, University of Texas, Austin, Tex., 198-212.

Viegas, D.X. and A.R.J. Borges (1986). "An Erosion Technique for the Measurement of the Shear Stress Field on a Flat Plate," Journal of Physics E: Scientific Instruments, 19(8):625-630.

TABLE 1. Details of Experiments

Δh (cm)	$R_o = \rho U_o\, d/\mu$ [1]	Measured quantities [2]	No. of Runs
15.2	2.3×10^4	ΔP_w, τ_o	2, 3
30.5	3.2×10^4	ΔP_w, τ_o	2, 3
45.7	4.0×10^4	ΔP_w, τ_o	2, 3
61.0	4.6×10^4	ΔP_w, τ_o	4, 6
91.4	5.6×10^4	ΔP_w, τ_o	2, 3
121.9	6.5×10^4	ΔP_w, τ_o	2, 3
152.4	7.2×10^4	ΔP_w, τ_o	2, 3
182.9	7.9×10^4	ΔP_w, τ_o	2, 3
203.2	8.4×10^4	ΔP_w, τ_o	2, 6

[1] ρ = density of the fluid, μ = Viscosity of fluid, U_o = velocity at the nozzle

[2] @ Radial Locations of 0.0, 0.5, 1.3, 2.0, 2.5, 3.0, 3.8, 6.4, 10.2, 21.6 cm